

Discrete Signal Processing on Graphs: Frequency Analysis

Aliaksei Sandryhaila, *Member, IEEE* and José M. F. Moura, *Fellow, IEEE*

Abstract—It is becoming increasingly important to work with datasets that arise not only from physical and engineering applications but from social, genetics, biomolecular, or many other domains. We recently introduced discrete signal processing on graphs that extends concepts and techniques from traditional signal processing and from algebraic signal processing to data indexed by arbitrary graphs. With time and image signals, low- and high-pass frequency components are naturally defined because frequencies can be ordered. But with signals defined on graphs there is no natural ordering of frequencies. This paper considers these concepts and defines low-, high-, and band-pass graph signals and graph filters by introducing a measure of the total variation of graph frequency components. We show how to design graph filters with specified frequency response and apply our methods to problems of sensor malfunctioning, regularization of graph signals, and classification of partially labeled data.

Keywords: Graph signal, graph filter, total variation, filter design, regularization, low pass, high pass, band pass.

I. INTRODUCTION

In our recent work [1], [2], [3], we have established a novel framework for the analysis and processing of datasets with complex structure that is usually represented by graphs. The framework, called *discrete signal processing on graphs* (DSP_G), views datasets as signals indexed by the nodes of a graph and formulates for them fundamental concepts of classical discrete signal processing theory (DSP), such as signal, shift, filter, spectrum, Fourier transform, impulse and frequency responses. DSP_G extends the classical DSP theory [4] for time signals and the algebraic signal processing theory for signals indexed by regular lattices [5], [6], [7], [8] and more general lattices [9], [10].

Signals indexed by graphs arise in many applications: preferences and opinions of individuals in social and economic networks [11], [12], [13]; research in collaborative activities, such as paper co-authorship and citations [14]; topics and relevance of documents in the World Wide Web interconnected by hyperlink references [15], [16]; measurements from sensor networks; interactions in molecular and gene regulatory networks; and many others.

DSP_G provides principled definitions to signal processing concepts that are difficult to formulate for graphs, such as shifts and filters on graphs and graph Fourier transform. The concepts of frequencies, spectral representations, and frequency response of filters are derived from the spectral

analysis of the graph shift introduced in [1]. In DSP, concepts like low- and high-frequency components of a signal have a clear and intuitive interpretation, since the frequency content of time series and digital images is described by complex or real sinusoids that oscillate at different rates. These oscillation rates provide the physical notion of “low” and “high” frequencies: low-frequency components oscillate less and high-frequency ones oscillate more. However, these concepts do not have an obvious interpretation in DSP_G . In fact, when signals are indexed by arbitrary graphs and not regular lattices, the graph signal frequency contents are characterized by the graph Fourier transform of the signal, where the graph Fourier transform matrix is obtained from the eigenvectors of the shift matrix (see Section II for details). It is no longer clear how to order frequencies to determine the low- or high-frequency contents of the graph signal. We address these issues by presenting a novel definition of total variation of graph signals. We show that total variation on graphs introduces a natural ordering for frequencies that we use to define low and high frequencies for signals on graphs, as well as the related notions of signal smoothness and low-, high-, and band-pass graph signals and filters. We illustrate these concepts with applications to sensor network analysis and data classification. We show that naturally occurring graph signals, such as measurements of physical quantities collected by sensor networks or class labels for datasets, are low-pass graph signals. We demonstrate that anomalies in graph signals arising as a result of sensor failures in sensor network data, which often correspond to unexpected variations in graph signals, may be detected using appropriately designed high-pass graph filters. Finally, we illustrate how to recover unknown low-frequency components of graph signals by applying a regularization technique on graphs.

Summary of the paper. In Section II, we present the notation and review the basics of DSP_G . In Section III, we give a novel definition of total variation of graph frequency components and use it to order frequencies, enabling us to introduce low-, high-, and band-pass signals. In Section IV, we discuss low-, high-, and band-pass filters and their design. In Section V, we illustrate these concepts with applications to malfunction detection in sensor networks and data classification, and provide experimental results with real-world datasets. Finally, Section VI concludes the paper.

II. DISCRETE SIGNAL PROCESSING ON GRAPHS

In this section, we briefly review notation and main concepts of the DSP_G framework that are relevant to our work in this

This work was supported in part by AFOSR grant FA95501210087. A. Sandryhaila and J. M. F. Moura are with the Department of Electrical and Computer Engineering, Carnegie Mellon University, Pittsburgh, PA 15213-3890. Ph: (412)268-6341; fax: (412)268-3890. Email: asandryh@andrew.cmu.edu, moura@ece.cmu.edu.

paper. A complete introduction to the theory can be found in [1], [2], [3].

A. Graph Signals

Signal processing on graphs is concerned with the analysis and processing of datasets in which data elements can be connected to each other according to some relational property. This relation is commonly expressed using a graph $G = (\mathcal{V}, \mathbf{A})$, where $\mathcal{V} = \{v_0, \dots, v_{N-1}\}$ is a set of nodes and \mathbf{A} is a weighted adjacency matrix of the graph. Each data element corresponds to node v_n (we also say the data element is indexed by v_n), and each weight $\mathbf{A}_{n,m}$ of a directed edge from v_m to v_n reflects the degree of relation of the m th data element to the n th one. Node v_m is an in-neighbor of v_n and v_n is an out-neighbor of v_m if $\mathbf{A}_{n,m} \neq 0$. If the graph is undirected, the relation goes both ways, $\mathbf{A}_{n,m} = \mathbf{A}_{m,n}$, and the nodes are neighbors.

Using this graph, we refer to the dataset as a *graph signal*, which is defined as a map from the set \mathcal{V} of nodes to the set of complex numbers \mathbb{C} :

$$\begin{aligned} \mathbf{s} &: \mathcal{V} \rightarrow \mathbb{C}, \\ v_n &\mapsto s_n. \end{aligned} \quad (1)$$

We assume that each dataset element s_n is a complex number. Since each signal is isomorphic to a complex-valued vector with N elements, we write graph signals as vectors

$$\mathbf{s} = (s_0 \quad s_1 \quad \dots \quad s_{N-1})^T \in \mathbb{C}^N.$$

However, we emphasize that each element s_n is *indexed* by node v_n of a given representation graph $G = (\mathcal{V}, \mathbf{A})$, as defined by (1). The space \mathcal{S} of graph signals (1) then is isomorphic to \mathbb{C}^N , and its dimension is $\dim \mathcal{S} = N$.

B. Graph Filters

In general, a *graph filter* is a system $\mathbf{H}(\cdot)$ that takes a graph signal \mathbf{s} as an input, processes it, and produces another graph signal $\tilde{\mathbf{s}} = \mathbf{H}(\mathbf{s})$ as an output.

A basic non-trivial filter defined on a graph $G = (\mathcal{V}, \mathbf{A})$, called the *graph shift*, is a local operation that replaces a data element s_n at node v_n with a linear combination of elements at the neighbors of node v_n . The output of the graph shift is given by the product of the input signal with the adjacency matrix of the graph:

$$\tilde{\mathbf{s}} = \mathbf{A}\mathbf{s}. \quad (2)$$

The shift is the basic building block in DSP_G , [1].

In this paper, we consider linear, shift-invariant graph filters. Filters are *linear* if for a linear combination of inputs they produce the same linear combination of outputs. Filters are *shift-invariant* if the result of consecutive processing of a signal by multiple graph filters does not depend on the order of processing; i.e., shift-invariant filters commute with each other. A linear, shift-invariant graph filter on a graph $G = (\mathcal{V}, \mathbf{A})$ is necessarily a polynomial in the adjacency matrix \mathbf{A} [1]:

$$h(\mathbf{A}) = h_0 \mathbf{I} + h_1 \mathbf{A} + \dots + h_L \mathbf{A}^L. \quad (3)$$

The output signal of the filter (3) is given by the matrix-vector multiplication:

$$\tilde{\mathbf{s}} = \mathbf{H}(\mathbf{s}) = h(\mathbf{A})\mathbf{s}.$$

Linear, shift-invariant graph filters possess a number of useful properties. They have at most $L \leq N_{\mathbf{A}}$ taps h_ℓ , where $N_{\mathbf{A}} = \deg m_{\mathbf{A}}(x)$ is the degree of the minimal polynomial¹ $m_{\mathbf{A}}(x)$ of \mathbf{A} . Furthermore, if a graph filter (3) is invertible, i.e., matrix $h(\mathbf{A})$ is non-singular, then its inverse is also a graph filter $g(\mathbf{A}) = h(\mathbf{A})^{-1}$ on the same graph $G = (\mathcal{V}, \mathbf{A})$. Finally, since addition and multiplication of graph filters produce new graph filters, the space of filters is an *algebra*, i.e., a vector space that is simultaneously a ring.

C. Graph Fourier Transform

In general, a Fourier transform performs the expansion of a signal into a *Fourier basis* of signals that are invariant to filtering. In the DSP_G framework, a graph Fourier basis corresponds to the Jordan basis of the graph adjacency matrix \mathbf{A} (the Jordan decomposition is reviewed in Appendix A). Following the DSP notation, distinct eigenvalues $\lambda_0, \lambda_1, \dots, \lambda_{M-1}$ of the adjacency matrix \mathbf{A} are called the *graph frequencies* and form the *spectrum* of the graph, and the Jordan eigenvectors that correspond to a frequency λ_m are called the *frequency components* corresponding to the m th frequency. Since multiple eigenvectors can correspond to the same eigenvalue, in general, a graph frequency can have multiple graph frequency components associated with it.

As reviewed in Appendix A, Jordan eigenvectors form the columns of the matrix \mathbf{V} in the Jordan decomposition (41)

$$\mathbf{A} = \mathbf{V} \mathbf{J} \mathbf{V}^{-1}.$$

Hence, the *graph Fourier transform* of a graph signal \mathbf{s} is calculated as

$$\hat{\mathbf{s}} = \mathbf{F} \mathbf{s}, \quad (4)$$

where $\mathbf{F} = \mathbf{V}^{-1}$ is the graph Fourier transform matrix. The values \hat{s}_n of the signal's graph Fourier transform (4) characterize the *frequency content* of the signal \mathbf{s} .

The *inverse graph Fourier transform* is given by

$$\mathbf{s} = \mathbf{F}^{-1} \hat{\mathbf{s}} = \mathbf{V} \hat{\mathbf{s}}. \quad (5)$$

It reconstructs the original signal from its frequency contents by constructing a linear combination of frequency components weighted by the signal's Fourier transform coefficients.

D. Frequency Response

The graph Fourier transform (4) also allows us to characterize the effect of the filter on the frequency content of an input signal. As follows from (3) and (4), as well as (41) in Appendix A,

$$\tilde{\mathbf{s}} = h(\mathbf{A})\mathbf{s} = \mathbf{F}^{-1} h(\mathbf{J}) \mathbf{F} \mathbf{s} \Leftrightarrow \mathbf{F} \tilde{\mathbf{s}} = h(\mathbf{J}) \hat{\mathbf{s}}. \quad (6)$$

¹The minimal polynomial of \mathbf{A} is the unique monic polynomial of the smallest degree that annihilates \mathbf{A} , i.e., $m_{\mathbf{A}}(\mathbf{A}) = 0$ [17], [18].



Fig. 1. Traditional graph representation for a finite discrete periodic time series of length N .

Hence, the frequency content of the output signal is obtained by multiplying the frequency content of the input signal by the block diagonal matrix

$$h(\mathbf{J}) = \begin{pmatrix} h(\mathbf{J}_{r_{0,0}}(\lambda_0)) & & & \\ & \ddots & & \\ & & \ddots & \\ & & & h(\mathbf{J}_{r_{M-1,D_{M-1}}}(\lambda_{M-1})) \end{pmatrix}.$$

We call this matrix the *graph frequency response* of the filter $h(\mathbf{A})$, and denote it as

$$\widehat{h(\mathbf{A})} = h(\mathbf{J}). \quad (7)$$

Notice that (6) extends the *convolution theorem* from classical signal processing [4] to graphs, since filtering a signal on a graph is equivalent in the frequency domain to multiplying the signal's spectrum by the frequency response of the filter.

E. Consistency with the Classical DSP

The DSP_G framework is consistent with the classical DSP theory. Finite (or periodic) time series is commonly represented by the directed cycle graph shown in Fig. 1, see [6], [1]. The direction of the edges represents the flow of time from past to future, and the edge from the last vertex v_{N-1} to v_0 captures the periodic signal extension $s_N = s_0$ for time series. The adjacency matrix of the graph in Fig. 1 is the $N \times N$ cyclic permutation matrix

$$\mathbf{A} = \mathbf{C}_N = \begin{pmatrix} & & & 1 \\ 1 & & & \\ & \ddots & & \\ & & \ddots & \\ & & & 1 \end{pmatrix}. \quad (8)$$

Substituting (8) into the graph shift (2) leads exactly to the time delay

$$\tilde{s}_n = s_{n-1 \bmod N}. \quad (9)$$

It is well known that the cyclic permutation (8) is diagonalizable, and its eigendecomposition, which coincides with the Jordan decomposition (41) is

$$\mathbf{C}_N = \frac{1}{N} \mathbf{DFT}_N^{-1} \begin{pmatrix} e^{-j\frac{2\pi \cdot 0}{N}} & & & \\ & \ddots & & \\ & & \ddots & \\ & & & e^{-j\frac{2\pi \cdot (N-1)}{N}} \end{pmatrix} \mathbf{DFT}_N, \quad (10)$$

where \mathbf{DFT}_N is the discrete Fourier transform matrix. Thus, as expected, the graph Fourier transform for signals indexed by the graph in Fig. 1 is $\mathbf{F} = \mathbf{DFT}_N$, and the corresponding frequencies are², for $0 \leq n < N$,

$$e^{-j\frac{2\pi}{N}n}. \quad (11)$$

²In DSP, the ratio $\frac{2\pi}{N}n$ in the exponent (11) sometimes is also referred to as frequency. In this case, the frequencies are N real numbers between 0 and 2π . However, to remain consistent with the discussion in this paper, we refer to the exponentials (11) as frequencies, and view them as complex numbers of magnitude 1 residing on the unit circle in the complex plane.

III. LOW AND HIGH FREQUENCIES ON GRAPHS

In this section, we introduce an ordering on graph frequencies that leads to the definition of low and high frequencies on graphs. It is based on the total variation of frequency components, which we also introduce. We demonstrate that the proposed ordering is unique for graphs with real spectra and not unique for graphs with complex spectra.

A. Total Variation on Graphs

In classical DSP, the *total variation* (TV) of a discrete signal is defined as the sum of magnitudes of differences between two consecutive signal samples [19], [20]:

$$\text{TV}(\mathbf{s}) = \sum_n |s_n - s_{n-1}|. \quad (12)$$

For a periodic time series $\mathbf{s} = (s_0, \dots, s_{N-1})^T$, the periodicity condition $s_n = s_{n \bmod N}$ leads to a modified definition

$$\text{TV}(\mathbf{s}) = \sum_{n=0}^{N-1} |s_n - s_{n-1 \bmod N}|. \quad (13)$$

The total variation (12) and (13) for time series or space signals, such as images, has a simple, intuitive interpretation: it compares how the signal varies with time or space. These concepts lie at the heart of many applications of DSP, including signal regularization and denoising [19], [20], image compression [21] and others.

The total variation function (13) compares two consecutive signal samples and calculates a cumulative magnitude of the signal change over time. Employing the concept of time shift, or delay, (9), we say that the total variation compares a signal \mathbf{s} to its shifted version: the smaller the difference between the original signal and the shifted one, the lower the signal's variation. Hence, we can write the expression (13) as

$$\text{TV}(\mathbf{s}) = \|\mathbf{s} - \mathbf{C}_N \mathbf{s}\|_1, \quad (14)$$

where \mathbf{C}_N is the cyclic shift matrix (8). With respect to the graph in Fig. 1 that represents a periodic time series, the total variation measures the difference between the signal values at each vertex and its neighbor.

Extending the expression (14) from the regular lattice to an arbitrary graph $G = (\mathcal{V}, \mathbf{A})$, we think of the total variation on a graph as a measure of similarity between a graph signal and its graph shifted version, i.e., between a graph signal and a weighted linear combination of its neighbors. Similarly to the total variation in DSP (13), the total variation on graphs measures how similar the signal value at each node is to the values at its neighboring nodes.

Definition 1 (Graph Total Variation): Let λ_{\max} denote the eigenvalue of \mathbf{A} with the largest magnitude, i.e.,

$$|\lambda_{\max}| \geq |\lambda_m| \quad (15)$$

for all $0 \leq m \leq M-1$. The *total variation on a graph* (TV_G) of a graph signal \mathbf{s} is defined as

$$\text{TV}_G(\mathbf{s}) = \frac{1}{\|\mathbf{s}\|_2} \left\| \mathbf{s} - \frac{1}{|\lambda_{\max}|} \mathbf{A} \mathbf{s} \right\|_2^2. \quad (16)$$

The normalization factor $1/|\lambda_{\max}|$ prevents the shifted signal from being scaled up due to the multiplication by \mathbf{A} , since it ensures that all eigenvalues of the shift matrix $\mathbf{A}/|\lambda_{\max}|$ have magnitude no greater than 1. Also, since the definition (16) of the total variation depends on the norm $\|\mathbf{s}\|_2$, we normalize the norm of the difference between the original and shifted signals in the numerator of (16) by the norm of the signal to facilitate the comparison of total variations for graph signals with different norms.

B. Variation of the Graph Fourier Basis

Next, using the total variation on graphs (16), we define an ordering of graph frequencies by calculating and comparing the variations of corresponding frequency components.

Recall from Section II that the graph Fourier basis is given by the Jordan basis of the adjacency matrix \mathbf{A} . Consider an eigenvalue λ of the adjacency matrix \mathbf{A} , and let $\mathbf{v} = \mathbf{v}_0, \mathbf{v}_1, \dots, \mathbf{v}_{R-1}$ be a Jordan chain of generalized eigenvectors that corresponds to this eigenvalue. Let the indicator function

$$i(r) = \begin{cases} 0, & r = 0 \\ 1, & 1 \leq r < R \end{cases}$$

specify whether \mathbf{v}_r is a proper eigenvector of \mathbf{A} or a generalized one. Then we can write the condition (37) on generalized eigenvectors (see Appendix A) as

$$\mathbf{A}\mathbf{v}_r = \lambda\mathbf{v}_r + i(r)\mathbf{v}_{r-1}. \quad (17)$$

Using (17), we write the total variation (16) of the generalized eigenvector \mathbf{v}_r as

$$\begin{aligned} \text{TV}_G(\mathbf{v}_r) &= \frac{1}{\|\mathbf{v}_r\|_2^2} \left\| \mathbf{v}_r - \frac{1}{|\lambda_{\max}|} \mathbf{A}\mathbf{v}_r \right\|_2^2 \quad (18) \\ &= \frac{1}{\|\mathbf{v}_r\|_2^2} \left\| \mathbf{v}_r - \frac{\lambda}{|\lambda_{\max}|} \mathbf{v}_r - \frac{i(r)}{|\lambda_{\max}|} \mathbf{v}_{r-1} \right\|_2^2 \\ &= \left| 1 - \frac{\lambda}{|\lambda_{\max}|} \right|^2 + \frac{i(r)^2}{|\lambda_{\max}|^2} \frac{\|\mathbf{v}_{r-1}\|_2^2}{\|\mathbf{v}_r\|_2^2} \\ &\quad - 2 \frac{i(r)}{|\lambda_{\max}|} \text{Re} \left(\left(1 - \frac{\lambda}{|\lambda_{\max}|} \right) \frac{\mathbf{v}_r^H \mathbf{v}_{r-1}}{\|\mathbf{v}_r\|_2^2} \right). \end{aligned}$$

In particular, when \mathbf{v}_r is a proper eigenvector of \mathbf{A} , i.e. $r = 0$ and $\mathbf{v}_r = \mathbf{v}$, the indicator function evaluates to $i(0) = 0$. In this case, it follows from (18) that the total variation of the eigenvector \mathbf{v} is

$$\text{TV}_G(\mathbf{v}) = \left| 1 - \frac{\lambda}{|\lambda_{\max}|} \right|^2. \quad (19)$$

Hence, when a frequency component is a proper eigenvector of the adjacency matrix \mathbf{A} , its total variation (19) is determined solely by the corresponding eigenvalue. In particular, all proper eigenvectors corresponding to the same eigenvalue have the same total variation. However, when a frequency component is not a proper eigenvector, we must use the expression (18) to calculate its variation to compare with other frequency components.

C. Frequency Ordering

The total variation of the Fourier basis, given by (18) and (19), allows us to order the graph frequency components in the order of increasing variation. Following DSP convention, we call frequency components with smaller variations *low* frequencies, while the ones with higher variations *high* frequencies.

Next, we determine the frequency ordering induced by the total variation (19) for graphs that have diagonalizable adjacency matrices, i.e., only have proper eigenvectors. These orderings can be similarly extended to graphs with non-diagonalizable adjacency matrices using the variation of generalized eigenvectors (18).

The following theorem establishes the relative ordering of two distinct real frequencies.

Theorem 1: Consider two distinct real eigenvalues $\lambda_m, \lambda_n \in \mathbb{R}$ of the adjacency matrix \mathbf{A} . Let \mathbf{v}_m and \mathbf{v}_n be the eigenvectors of \mathbf{A} corresponding to these eigenvalues. If the eigenvalues are ordered as

$$\lambda_m < \lambda_n, \quad (20)$$

then the total variations of the corresponding eigenvectors satisfy

$$\text{TV}_G(\mathbf{v}_m) > \text{TV}_G(\mathbf{v}_n). \quad (21)$$

Proof: Since the eigenvalues are real, the difference between the total variations of the two eigenvectors is

$$\begin{aligned} &\text{TV}_G(\mathbf{v}_m) - \text{TV}_G(\mathbf{v}_n) \\ &= \left| 1 - \frac{\lambda_m}{|\lambda_{\max}|} \right|^2 - \left| 1 - \frac{\lambda_n}{|\lambda_{\max}|} \right|^2 \\ &= 1 - 2 \frac{\lambda_m}{|\lambda_{\max}|} + \frac{\lambda_m^2}{|\lambda_{\max}|^2} - 1 + 2 \frac{\lambda_n}{|\lambda_{\max}|} - \frac{\lambda_n^2}{|\lambda_{\max}|^2} \\ &= \frac{\lambda_m - \lambda_n}{|\lambda_{\max}|^2} (\lambda_m + \lambda_n - 2|\lambda_{\max}|). \quad (22) \end{aligned}$$

It follows from (20) that

$$\lambda_m - \lambda_n < 0.$$

Furthermore, it follows the definition (15) of λ_{\max} that

$$\lambda_m + \lambda_n - 2|\lambda_{\max}| < 0.$$

Hence, the difference (22) between the total variations satisfies

$$\text{TV}_G(\mathbf{v}_m) - \text{TV}_G(\mathbf{v}_n) > 0,$$

which is equivalent to (21). \blacksquare

As follows from Theorem 1, if a graph has a real spectrum and its frequencies satisfy

$$\lambda_0 > \lambda_1 > \dots > \lambda_{M-1}, \quad (23)$$

then λ_0 represents the lowest frequency, while λ_{M-1} is the highest frequency. Moreover, the arrangement (23) is a unique ordering of all frequencies from lowest to highest. This frequency ordering for matrices with real spectra is visualized in Fig. 2(a).

The next theorem extends Theorem 1 and establishes the relative ordering of two distinct frequencies corresponding to complex eigenvalues.

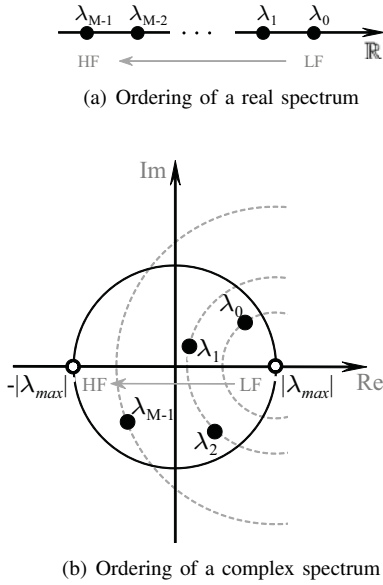


Fig. 2. Frequency ordering from low frequencies (LF) to high frequencies (HF) for graphs with real and complex spectra.

Theorem 2: Consider two distinct complex eigenvalues $\lambda_m, \lambda_n \in \mathbb{C}$ of the adjacency matrix \mathbf{A} . Let \mathbf{v}_m and \mathbf{v}_n be the eigenvectors of \mathbf{A} corresponding to these eigenvalues. The total variations of the corresponding eigenvectors are related as

$$\text{TV}_G(\mathbf{v}_m) < \text{TV}_G(\mathbf{v}_n), \quad (24)$$

if the eigenvalue λ_m is located closer to the value $|\lambda_{\max}|$ on the complex plane than the eigenvalue λ_n .

Proof: This result follows immediately from the interpretation of the total variation (19) as a distance function. Since \mathbf{A} is not a zero matrix, the eigenvalue $\lambda_{\max} \neq 0$. Then, multiplying both sides of the inequality (24) by $|\lambda_{\max}|^2$ yields the inequality

$$\left| |\lambda_{\max}| - \lambda_m \right|^2 < \left| |\lambda_{\max}| - \lambda_n \right|^2. \quad (25)$$

The expressions on each side of the inequality (25) are precisely the distances from λ_m and λ_n to $|\lambda_{\max}|$ on the complex plane. ■

As follows from Theorem 2, frequencies of a graph with a complex spectrum are ordered by their distance from $|\lambda_{\max}|$. As a result, in contrast to the graphs with real spectra, distinct complex frequencies can yield the same total variation for their corresponding frequency components, since all eigenvalues lying on a circle of radius ρ centered at point $|\lambda_{\max}|$ on the complex plane have the same total variation $\rho/|\lambda_{\max}|^2$. Thus, the induced ordering of complex frequencies from lowest to highest is not unique.

The frequency ordering for matrices with complex spectra is visualized in Fig. 2(b). Notice that, by definition (15) of λ_{\max} , all graph frequencies λ_m can lie only inside and on the boundary of the circle with radius $|\lambda_{\max}|$.

Consistency with DSP theory. The proposed frequency ordering for arbitrary graphs is consistent with the classical DSP theory. Recall from (10) that the cycle graph in Fig. 1,

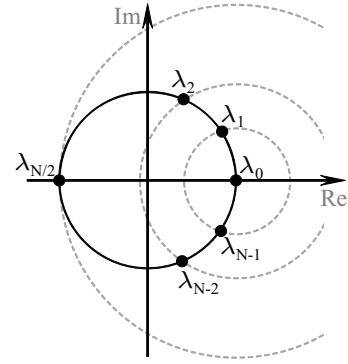


Fig. 3. Frequency ordering for finite discrete periodic time series. Frequencies λ_m and λ_{N-m} have the same total variations since they lie on the same circle centered around 1.

which represents periodic time series, has a complex spectrum

$$\lambda_n = e^{-j\frac{2\pi}{N}n}$$

for $0 \leq n < N$. Hence, the total variation of the n th frequency component is

$$\begin{aligned} \text{TV}_G(\mathbf{v}_n) &= \left| 1 - e^{-j\frac{2\pi n}{N}} \right|^2 \\ &= \left(1 - \cos \frac{2\pi n}{N} \right)^2 + \sin^2 \frac{2\pi n}{N} \\ &= 2 - 2 \cos \frac{2\pi n}{N}. \end{aligned}$$

It follows that the frequencies λ_m and λ_{N-m} have the same variation, and the induced order from lowest to highest frequencies is $\lambda_0, \lambda_1, \lambda_{N-1}, \lambda_2, \lambda_{N-2}, \dots$, with the lowest frequency corresponding to $\lambda_0 = 1$ and the highest frequency corresponding to $\lambda_{N/2} = -1$ for even N or $\lambda_{(N\pm 1)/2}$ for odd N . This ordering is visualized in Fig. 3, and it is the conventional frequency ordering for time series [4].

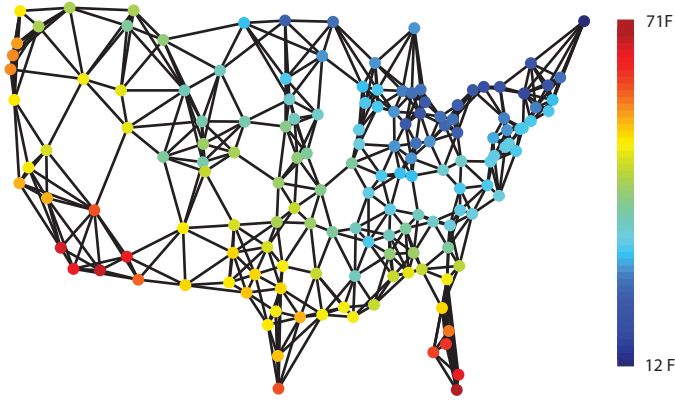
D. Smoothness of Graph Signals

Signal *smoothness* is a relative, qualitative measure of how much a signal varies with respect to the underlying indexing graph. We can call a signal smooth, if its variation (16) is low relative to other graph signals. Alternatively, a signal can be called smooth if most of its energy is concentrated in the low frequencies, i.e., smooth signals are low-frequency signals.

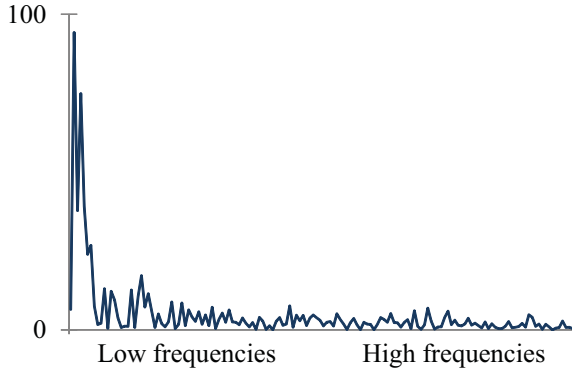
Let us illustrate the concept of smoothness with an example. Consider a network of 150 weather stations that measure daily temperature near major cities across the United States [22]. We construct the graph representing these 150 temperature measurements as a 6-nearest neighbor graph, in which every sensor corresponds to a vertex and connects to six closest weather stations. If vertices v_n and v_m are connected, the weight of the corresponding edge is assigned as

$$\mathbf{A}_{n,m} = \frac{e^{-d_{nm}^2}}{\sqrt{\sum_{k \in \mathcal{N}_n} e^{-d_{nk}^2} \sum_{\ell \in \mathcal{N}_m} e^{-d_{m\ell}^2}}}. \quad (26)$$

where \mathcal{N}_n denotes the neighborhood of the vertex v_n , i.e., the indices of all its neighbors; and $d_{n,m}$ denotes the geodesical



(a) Temperature on February 1, 2003



(b) Magnitudes of the graph Fourier transform coefficients

Fig. 4. Example temperature measured by 150 weather stations across the United States on February 1, 2003. Its frequency content indicates that the measurements form a smooth signal on the graphs of sensors; i.e., the graph signal is low-pass.

distance between the n th and m th stations. A daily snapshot of all temperatures forms a signal indexed by this graph.

Fig. 4(a) shows the temperature measured by this weather station network on February 1, 2003. The total variation of this graph signal is 0.08. The frequency content of this signal is shown in Fig. 4(b); it has most of its high-magnitude coefficients concentrated in the low frequencies. Hence, this signal is a low-frequency signal, and it can be considered smooth.

Using the construction of the graph as well as studying the measurements in Fig. 4(a) directly, we can interpret the smoothness of the signal in this example as the property that the temperatures in connected cities, i.e., cities located close to each other, are similar. In Section V-A, we demonstrate how this interpretation can lead to the detection of malfunctioning sensors.

IV. FILTER DESIGN

Analysis of low and high frequencies present in a graph signal provides important information about the signal's behavior on the graph. When a signal is processed with a graph filter, its frequency content changes according to the frequency response (7) of the filter. Similar to classical DSP, we can

characterize graph filters as low-, high-, and band-pass filters based on the structure of their frequency response.

A. Low-, High-, and Band-pass Graph Filters

Filters are *low-pass* if they do not significantly affect the frequency content of low-frequency signals but attenuate, i.e., reduce, the magnitude of high-frequency signals. Analogously, *high-pass* filters pass high-frequency signals while attenuating low-frequency ones, and *band-pass* filters pass signals with frequency content within a specified frequency band while attenuating all others.

As demonstrated by (6), the action of a graph filter $h(\mathbf{A})$ of the form (3) on the frequency content of a graph signal \mathbf{s} is completely specified by its frequency response (7). For simplicity of presentation, we discuss here graphs with diagonalizable adjacency matrices, for which (7) is a diagonal matrix with $h(\lambda_m)$ on the main diagonal, $0 \leq m < M$. In this case, the Fourier transform coefficients of the filtered signal

$$\tilde{\mathbf{s}} = h(\mathbf{A})\mathbf{s}$$

are the Fourier transform coefficients of the input signal multiplied element-wise by the frequency response of the filter, i.e.,

$$\mathbf{F}\tilde{\mathbf{s}} = \begin{pmatrix} h(\lambda_0) & & \\ & \ddots & \\ & & h(\lambda_{M-1}) \end{pmatrix} \hat{\mathbf{s}} = \begin{pmatrix} h(\lambda_0)\hat{s}_0 \\ \vdots \\ h(\lambda_{M-1})\hat{s}_{N-1} \end{pmatrix}.$$

Hence, to attenuate signals with frequency content lying inside a specific part of the spectrum, we should select, or design, a filter $h(\mathbf{A})$ that for corresponding frequencies λ_m satisfies $h(\lambda_m) \approx 0$.

Consider an example of ideal low-pass and high-pass filters $h(\mathbf{A})$ and $g(\mathbf{A})$. Let the cut-off frequency λ_{cut} equal to the median of the bandwidth, i.e., be such that exactly half of frequencies λ_m are lower frequencies than λ_{cut} . The frequency responses of these filters are defined as

$$h(\lambda_m) = 1 - g(\lambda_m) = \begin{cases} 1, & \lambda_m > \lambda_{\text{cut}}, \\ 0, & \lambda_m \leq \lambda_{\text{cut}}. \end{cases} \quad (27)$$

As we demonstrate next, the design of such filters, as well as any low-, high-, and band-pass graph filters, is a linear problem.

B. Frequency Response Design for Graph Filters

We can specify a graph filter through its frequency response $h(\lambda_m)$ at its distinct frequencies λ_m , $m = 0, \dots, M-1$. As we discussed in Section II, graph filters (3) are polynomials of degree smaller than $N_{\mathbf{A}}$, where $N_{\mathbf{A}}$ is the degree of the minimal polynomial of \mathbf{A} . Hence, they can have up to $N_{\mathbf{A}}$ coefficients h_ℓ . We can design a filter with a frequency response specified by $h(\lambda_m) = \alpha_m$ by solving a system of M linear equations with $N_{\mathbf{A}}$ unknowns $h_0, \dots, h_{N_{\mathbf{A}}-1}$:

$$\begin{aligned} h_0 + h_1\lambda_0 + \dots + h_{N_{\mathbf{A}}-1}\lambda_0^{N_{\mathbf{A}}-1} &= \alpha_0, \\ h_0 + h_1\lambda_1 + \dots + h_{N_{\mathbf{A}}-1}\lambda_1^{N_{\mathbf{A}}-1} &= \alpha_1, \\ &\vdots \\ h_0 + h_1\lambda_{M-1} + \dots + h_{N_{\mathbf{A}}-1}\lambda_{M-1}^{N_{\mathbf{A}}-1} &= \alpha_{M-1}. \end{aligned} \quad (28)$$

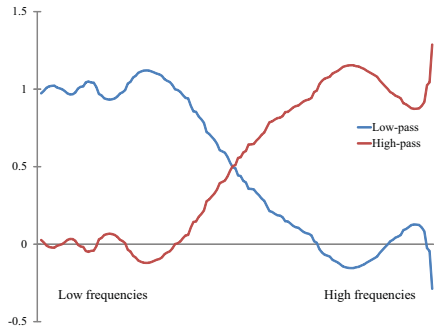


Fig. 5. Frequency responses of low-pass and high-pass filters for the sensor graph in Fig. 4(a). The length of the filters is restricted to 10 coefficients.

This system can be rewritten as

$$\begin{bmatrix} 1 & \lambda_0 & \dots & \lambda_0^{N_{\mathbf{A}}-1} \\ 1 & \lambda_1 & \dots & \lambda_1^{N_{\mathbf{A}}-1} \\ \vdots & \vdots & \ddots & \vdots \\ 1 & \lambda_{M-1} & \dots & \lambda_{M-1}^{N_{\mathbf{A}}-1} \end{bmatrix} \begin{bmatrix} h_0 \\ h_1 \\ \vdots \\ h_{N_{\mathbf{A}}-1} \end{bmatrix} = \begin{bmatrix} \alpha_0 \\ \alpha_1 \\ \vdots \\ \alpha_{M-1} \end{bmatrix}. \quad (29)$$

The system matrix in (29) is a Vandermonde matrix. The degree $N_{\mathbf{A}}$ of the minimal polynomial is always greater or equal to the number M of distinct eigenvalues, i.e., $N_{\mathbf{A}} \geq M$ [17], [18]. Hence, the Vandermonde matrix has full rank, and a filter with the desired frequency response (28) can always be designed. The equality $N_{\mathbf{A}} = M$ is achieved only if the adjacency matrix \mathbf{A} is diagonalizable. In this case, there exists exactly one solution to the system (28). Otherwise, the system is underdetermined and can have multiple solutions, i.e., multiple filters can have the same frequency response.

On the other hand, we may want to restrict the number of coefficients in the graph filter, for example, for the purposes of computational efficiency or numerical stability. In this case, the system may become overdetermined and will not have an exact solution. Instead, we will have to find an approximate solution.

As an example, consider the ideal low-pass and high-pass filters $h(\mathbf{A})$ and $g(\mathbf{A})$ specified by (27). The filter coefficients h_ℓ are obtained from (28) by setting α_m to 1 for frequencies lower than λ_{cut} and to 0 otherwise; and vice versa for g_ℓ . Since the solution to this system of equations can be prone to numerical errors, we may want to restrict the length of the filters to $L \ll N_{\mathbf{A}}$ coefficients, i.e., require that $h(\mathbf{A})$ and $g(\mathbf{A})$ are polynomials of degree $L - 1 \ll N_{\mathbf{A}}$, and find low- and high-pass filters that best approximate the ideal filters in the least-squares sense. Fig. 5 shows the frequency responses for low- and high-pass filters with $L = 10$ coefficients for the sensor graph in Fig. 4(a), where $N_{\mathbf{A}} = 150$. By design, the constructed filters satisfy the relation [23]

$$h(\mathbf{A}) = \mathbf{I}_N - g(\mathbf{A}). \quad (30)$$

If we require that $h(\mathbf{A})$ and $g(\mathbf{A})$ do not have the same number of coefficients or if we use an approximation metric other than least squares, the constructed polynomials will not satisfy (30).

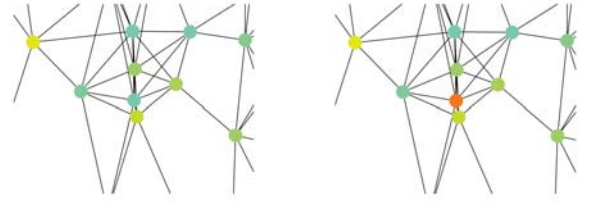


Fig. 6. A subgraph of the sensor graph in Fig. 4(a) showing the (a) true and (b) corrupted measurement by the sensor located in Colorado Springs, CO.

V. APPLICATIONS

In this section, we apply the theory discussed in this paper to graphs and datasets that arise in different contexts. We demonstrate how the $\text{DSP}_{\mathbf{G}}$ framework allows us to take advantage of such standard signal processing techniques as band-pass filtering and signal regularization to solve interesting problems from sensor networking and data classification.

A. Malfunction Detection in Sensor Networks

Today, sensors are ubiquitous. They are usually cheap to manufacture and deploy, so networks of sensors are used to measure and monitor a wide range of physical quantities from structural integrity of buildings to air pollution. However, the sheer quantity of sensors and the area of their deployment may make it challenging to check that every sensor is operating correctly. As an alternative, it is desirable to detect a malfunctioning sensor solely from the data it generates. We illustrate here how the $\text{DSP}_{\mathbf{G}}$ framework can be used to devise a simple solution to this problem.

Many physical quantities represent smooth signals with respect to graphs of sensors they are measured with. As an illustration, consider the temperature across the United States measured by 150 weather stations located near major cities [22]. An example temperature measurement was already shown in Fig. 4(a), and the construction of the corresponding weather station graph was discussed in Section III-D. The graph Fourier transform of this temperature snapshot is shown in Fig. 4(b), with frequencies ordered from lowest to highest. Most of the signal's energy is concentrated in the low frequencies, i.e., the signal varies slowly across the graph and so it is a smooth graph signal. As we discussed in Section III-D, the smooth nature of the temperature graph signal has the meaning of spatial smoothness, i.e., that cities located close to each other have similar temperatures.

A sensor malfunction may cause an unusual difference between its measurements and the measurements of nearby stations. Fig. 6 shows an example of an (artificially) corrupted measurement, where the station located near Colorado Springs, CO, reports a measurement that contains an error of 20 degree Fahrenheit (temperature at each sensor is color-coded using the same color scheme as in Fig. 4(a)). The true measurement in Fig. 6(a) is very similar to measurements at neighboring cities, while the corrupted measurement in Fig. 6(b) differs significantly from its neighbors.

The net effect of such difference is to make the graph signal less smooth; this is reflected in the signal's graph Fourier

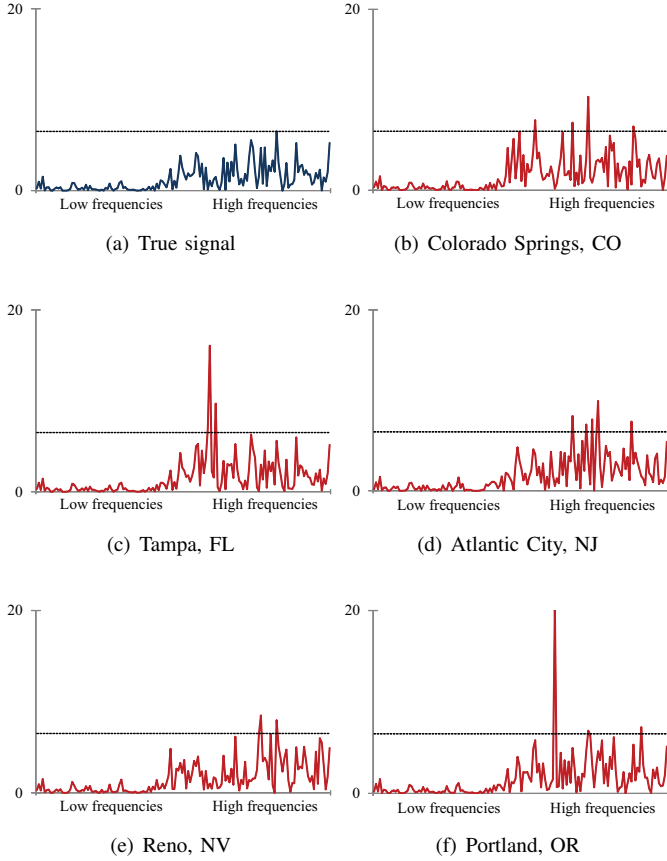


Fig. 7. The magnitudes of spectral coefficients of the original and corrupted temperature measurements after high-pass filtering: (a) the true signal from Fig. 4(a); (b)-(f) signals obtained from the true signal by corrupting the measurement of a single station located at the indicated city.

transform that has larger magnitudes at higher frequencies. By high-pass filtering the signal and then thresholding the filtered output, we can detect such anomaly and, hence, the corresponding sensor malfunction.

Experiments. We consider the detection of a single corrupted temperature station. We simulate the malfunctioning by corrupting the sensor’s measurement by 20 degrees Fahrenheit; such an error is small, so that the reported measurement is still within reasonable bounds and is hard to detect by direct inspection of the measurement of each station separately. To detect the malfunction, we extract the high-frequency component of the resulting graph signal using the high-pass filter constructed in Section IV-B and shown in Fig. 5 and threshold it. If one or more Fourier transform coefficients exceeds the threshold value, we conclude that a sensor is malfunctioning.

Results. Fig. 7 shows the frequency contents of high-pass filtered signals that contain a corrupted measurement from a sensor at five different locations. A comparison with the high-pass component of the uncorrupted signal in Fig. 7(a) demonstrates coefficients above thresholds that lead to the detection of a corrupted signal.

B. Data Classification

Data classification is an important problem in machine learning and data mining [24], [25]. Its objective is to classify each element of the dataset based on specified characteristics of the data. For example, image and video databases may be classified based on their contents; documents are grouped with respect to their topics; and customers may be distinguished based on their shopping preferences. In all cases, each dataset element is assigned a label, from a pre-defined group of labels, that assigns the element to a class.

Large datasets often cannot be classified manually. In this case, a common approach is to classify only a subset of elements and then use a known structure of the dataset to predict the labels for the remaining elements. A key assumption in this approach is that similar elements tend to be in the same class. Hence, knowledge of similarity between dataset elements provides means for inferring unknown labels from known ones. In this case, the labels tend to form a smooth signal over the graph of similarities.

Consider a graph $G = (\mathcal{V}, \mathbf{A})$ with N vertices that represent N data elements. We assume that two elements are similar to each other if the corresponding vertices are connected; if their connection is directed, the similarity is assumed only in the direction of the edge. We define a signal $\mathbf{s}^{(known)}$ on this graph that captures known labels. For a two-class problem, this signal is defined as

$$s_n^{(known)} = \begin{cases} +1, & n\text{th element belongs to class 1,} \\ -1, & n\text{th element belongs to class 2,} \\ 0, & \text{class is unknown.} \end{cases}$$

The predicted labels for all data elements are found as the smoothest signal on the graph $G = (\mathcal{V}, \mathbf{A})$ that preserves known labels. That is, we define the predicted labels as the solution to the optimization problem

$$\mathbf{s}^{(predicted)} = \underset{\mathbf{s} \in \mathbb{R}^N}{\operatorname{argmin}} \operatorname{TV}_G(\mathbf{s}) \quad (31)$$

subject to

$$\|\mathbf{C} \mathbf{s}^{(known)} - \mathbf{C} \mathbf{s}\|_2^2 < \epsilon, \quad (32)$$

where \mathbf{C} is a $N \times N$ diagonal matrix such that

$$C_{n,n} = \begin{cases} 1, & \text{if } s_n^{(known)} \neq 0, \\ 0, & \text{otherwise.} \end{cases}$$

The parameter ϵ in (32) controls how well the known labels are preserved.

Alternatively, the problem (31) with condition (32) can be formulated and solved as

$$\mathbf{s}^{(predicted)} = \underset{\mathbf{s} \in \mathbb{R}^N}{\operatorname{argmin}} (\operatorname{TV}_G(\mathbf{s}) + \alpha \|\mathbf{C} \mathbf{s}^{(known)} - \mathbf{C} \mathbf{s}\|_2^2). \quad (33)$$

Here, the parameter α controls the relative importance of conditions (31) and (32).

Once the predicted signal $\mathbf{s}^{(predicted)}$ is calculated, the unlabeled data elements are assigned to class 1 if $s_n^{(predicted)} > 0$ and another class otherwise.

In signal processing, approaches based on the minimization of the total variation for time series (13) are called *regularization*. They have been used for signal denoising, deblurring and recovery [26], [27], [28], [29]. In data classification, approaches based on solving minimization problems similar to (31) and (33) have been considered in [30], [31], [25], [32]. However, these works used a different signal variation function that was based on the Laplacian matrix of the graph. The Laplacian matrix for a graph $G = (\mathcal{V}, \mathbf{A})$ is the $N \times N$ matrix

$$\mathbf{L} = \mathbf{D} - \mathbf{A},$$

where \mathbf{D} is a diagonal matrix with diagonal elements given by

$$\mathbf{D}_{n,n} = \sum_{m=0}^{N-1} \mathbf{A}_{n,m}.$$

The corresponding graph signal variation function based on the Laplacian matrix is defined as

$$\text{TV}_L(\mathbf{s}) = \mathbf{s}^T \mathbf{L} \mathbf{s}. \quad (34)$$

The variation function (34) has been partially inspired by works in spectral graph theory [33] and machine learning on graphs [34], [35], and recently has been proposed for signal analysis on graphs [36], [37], [38], [39], [40]. The use of the Laplacian matrix assumes, implicitly or explicitly, that the graph that represents the data is a *similarity* or *homophilic* graph. In such graphs, nodes are connected by *undirected* edges with real non-negative edge weights that reflect the degree of similarity between data elements, i.e., the larger the weight the more similar the corresponding two elements are. However, many real-world datasets are represented by graphs that do not satisfy these restrictions and have directed edges and/or negative or complex edge weights. In contrast, our definition of graph signal variation (16) applies to arbitrary graphs and does not make any of these restrictive assumptions.

Experiments. We illustrate the application of graph signal regularization to data classification by solving the minimization problem (33) for two datasets; in both cases we set the value of the parameter α to 1.

The first dataset is a collection of images of handwritten digits 0 and 1 [41]. For each digit, we have 1000 grayscale images of size 28×28 . The graph is constructed by viewing each image as a point in a $28^2 = 784$ -dimensional vector space, computing Euclidean distances between all images, and connecting each image with six nearest neighbors.

For edge weights, we experiment with weighted and unweighted graphs. In the first case, when two images are connected, we assign the weight

$$\mathbf{A}_{n,m} = e^{-d_{n,m}^2} \quad (35)$$

to the corresponding edge, where $d_{n,m}$ is the Euclidean distance between the images. In the second case, we assign the edge weight to be $\mathbf{A}_{n,m} = 1$. By considering two cases, we evaluate the relevance of similarity information on the accuracy of classification based on graph signal regularization.

The second dataset is a collection of 1224 online political blogs [15]. These blogs can be either “conservative” or “liberal.” The corresponding graph represents blogs as vertices

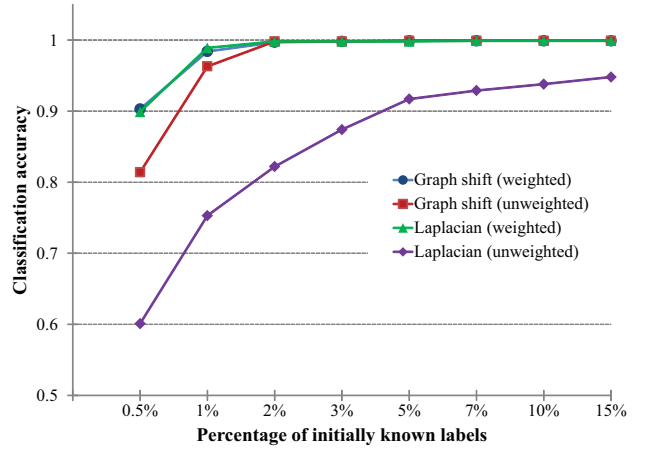


Fig. 8. Classification accuracy of images of handwritten digits 0 and 1 using the graph shift-based regularization and Laplacian-based regularization on weighted and unweighted similarity graphs.

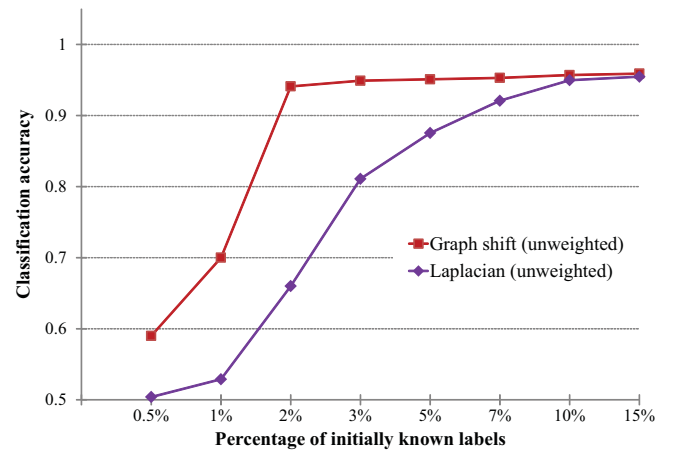


Fig. 9. Classification accuracy of political blogs using the graph shift-based regularization and Laplacian-based regularization on an unweighted graph of hyperlink references.

and hyperlink references between blogs as edges between corresponding vertices. In contrast to the previous dataset, in this case we only have access to the unweighted graph, since we cannot assign a similarity value to the hyperlink.

For both datasets, we classify between 0.5% and 15% of randomly selected datasets, and then measure the accuracy of classification of remaining elements. Results of each test are averaged over 100 runs.

For comparison, we also consider the Laplacian-based total variation function (34), and solve the minimization problem

$$\mathbf{s}^{(\text{predicted})} = \underset{\mathbf{s} \in \mathbb{R}^N}{\text{argmin}} \left(\text{TV}_L(\mathbf{s}) + \alpha \| \mathbf{C}(\mathbf{s}^{(\text{known})} - \mathbf{s}) \|_2^2 \right), \quad (36)$$

where we set α to 1 as well.

Results. Average classification accuracies for image and blog datasets are shown, respectively, in Fig. 8 and Fig. 9.

When we use the weighted graph to represent images, signal regularization solutions (33) and (36) based on, respectively, the total variation (16) and Laplacian variation (34), perform

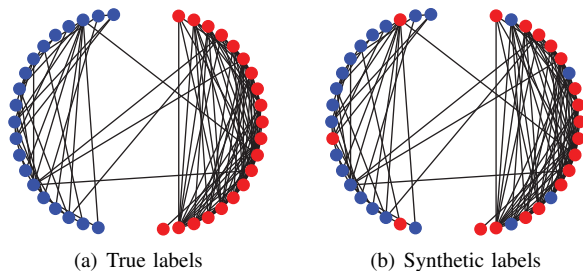


Fig. 10. A subgraph of 40 blogs labels: blue corresponds to “liberal” blogs and red corresponds to “conservative” ones. Labels in (a) form a smoother graph signal than labels in (b).

equally well and produce classification accuracies above 99% with only 2% of initially known labels. However, for the unweighted graph, the regularization (33) is significantly more accurate than the Laplacian-based regularization (36): it still achieves the accuracy over 99% with only 2% of initially known labels. This result demonstrates that the Laplacian-based approach suffers when the similarity information between data elements is not available, while the DSP_G -based approach is robust to the absence of such information.

Similar results are obtained for the blogs dataset. Here, the regularization solution (33) achieves accuracy close to 96% with only 2% of initially labeled blogs, while the solution (36) requires 15% of labels to be known initially to achieve the same level of accuracy.

Discussion. We illustrate how classification based on signal regularization works. Fig. 10 shows a subgraph of 40 blogs with their mutual hyperlinks randomly extracted from the entire dataset. Fig. 10(a) contains true labels for these blogs obtained from [15], while the labels in Fig. 10(b) are obtained by randomly switching 7 out of 40 labels. The frequency content of the true and synthetic labels as signals on this subgraph, shown in Fig. 11, indicate that the true labels form a smoother signal than the synthetic ones. This observation supports our assumption that the smoothest solution to the regularization problem (33) should correspond to correct label assignment.

Incidentally, this assumption also explains why the maximum classification accuracy achieved in our experiments is 96%, as seen in Fig. 9. We expect that every blog contains more hyperlinks to blogs of its own type than to blogs of the opposite type. However, after inspecting the entire dataset, we discovered that 50 blogs out of 1224, i.e., 4% of the total dataset, do not obey this assumption. As a result, 4% of all blogs are always misclassified, which results in maximum achievable accuracy of 96%.

VI. CONCLUSIONS

This paper introduces low-, high-, and band-pass signals and low-, high-, and band-pass filters on graphs. These concepts do not have simple and intuitive interpretations for arbitrary graphs. We define them using the concept of frequencies in digital signal processing on graphs (DSP_G). We propose a novel definition of a total variation on graphs that measures the difference between a graph signal and its shifted version. We

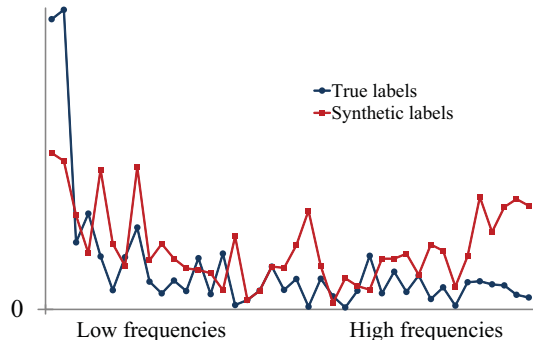


Fig. 11. Magnitudes of the spectral coefficients for graph signals formed by true and synthetic labels in Fig. 10.

use the total variation on graphs to order graph frequencies and to define low- and high-pass graph signals and filters. We design filters with specified desired frequency response by finding least squares approximations to solutions of systems of linear algebraic equations. We use these concepts and methodologies in sensor network analysis and data classification, and apply them to real-world datasets of temperature measurements collected by a sensor network, images, and online documents. Our experimental results show that the techniques presented in this paper are promising in problems like detecting sensor malfunctions, graph signal regularization, and classification of partially labeled data.

APPENDIX A: JORDAN DECOMPOSITION

An arbitrary matrix $\mathbf{A} \in \mathbb{C}^{N \times N}$ has $M \leq N$ distinct eigenvalues $\lambda_0, \dots, \lambda_{M-1}$. Each eigenvalue λ_m has D_m corresponding eigenvectors $\mathbf{v}_{m,0}, \dots, \mathbf{v}_{m,D_m-1}$ that satisfy

$$(\mathbf{A} - \lambda_m \mathbf{I}_N) \mathbf{v}_{m,d} = 0.$$

Moreover, each eigenvector $\mathbf{v}_{m,d}$ can generate a *Jordan chain* of $R_{m,d} \geq 1$ *generalized eigenvectors* $\mathbf{v}_{m,d,r}$, $0 \leq r < R_{m,d}$, where $\mathbf{v}_{m,d,0} = \mathbf{v}_{m,d}$, that satisfy

$$(\mathbf{A} - \lambda_m \mathbf{I}) \mathbf{v}_{m,d,r} = \mathbf{v}_{m,d,r-1}. \quad (37)$$

All eigenvectors and corresponding generalized eigenvectors are linearly independent.

For each eigenvector $\mathbf{v}_{m,d}$ and its Jordan chain of size $R_{m,d}$, we define a *Jordan block* matrix of dimensions $R_{m,d} \times R_{m,d}$ as

$$J_{R_{m,d}}(\lambda_m) = \begin{pmatrix} \lambda_m & 1 & & \\ & \lambda_m & \ddots & \\ & & \ddots & 1 \\ & & & \lambda_m \end{pmatrix} \in \mathbb{C}^{R_{m,d} \times R_{m,d}}. \quad (38)$$

By construction, each eigenvalue λ_m is associated with D_m Jordan blocks, each of dimension $R_{m,d} \times R_{m,d}$, where $0 \leq d < D_m$. Next, for each eigenvector $\mathbf{v}_{m,d}$, we collect its Jordan chain into a $N \times R_{m,d}$ matrix

$$\mathbf{V}_{m,d} = (\mathbf{v}_{m,d,0} \quad \dots \quad \mathbf{v}_{m,d,R_{m,d}-1}). \quad (39)$$

We concatenate all blocks $\mathbf{V}_{m,d}$, $0 \leq d < D_m$ and $0 \leq m < M$, into one block matrix

$$\mathbf{V} = (\mathbf{V}_{0,0} \quad \dots \quad \mathbf{V}_{M-1,D_{M-1}}), \quad (40)$$

so that the block $\mathbf{V}_{m,d}$ is at position $\sum_{k=0}^{m-1} D_k + d$ in this matrix. Then matrix \mathbf{A} is written in its *Jordan decomposition* form as

$$\mathbf{A} = \mathbf{V} \mathbf{J} \mathbf{V}^{-1}, \quad (41)$$

where the block-diagonal matrix

$$\mathbf{J} = \begin{pmatrix} \mathbf{J}_{R_{0,0}}(\lambda_0) & & \\ & \ddots & \\ & & \mathbf{J}_{R_{M-1,D_{M-1}}}(\lambda_{M-1}) \end{pmatrix} \quad (42)$$

is called the *Jordan normal form* of \mathbf{A} . The columns of \mathbf{V} , i.e., all eigenvectors and generalized eigenvectors of \mathbf{A} , are called the *Jordan basis* of \mathbf{A} .

REFERENCES

- [1] A. Sandryhaila and J. M. F. Moura, "Discrete signal processing on graphs," *IEEE Trans. Signal Proc.*, vol. 61, no. 7, pp. 1644–1656, 2013.
- [2] A. Sandryhaila and J. M. F. Moura, "Discrete signal processing on graphs: Graph Fourier transform," in *Proc. IEEE Int. Conf. Acoust., Speech and Signal Proc.*, 2013.
- [3] A. Sandryhaila and J. M. F. Moura, "Discrete signal processing on graphs: Graph filters," in *Proc. IEEE Int. Conf. Acoust., Speech and Signal Proc.*, 2013.
- [4] A. V. Oppenheim, R. W. Schaffer, and J. R. Buck, *Discrete-Time Signal Processing*, Prentice Hall, 2nd edition, 1999.
- [5] M. Püschel and J. M. F. Moura, "The algebraic approach to the discrete cosine and sine transforms and their fast algorithms," *SIAM J. Comp.*, vol. 32, no. 5, pp. 1280–1316, 2003.
- [6] M. Püschel and J. M. F. Moura, "Algebraic signal processing theory: Foundation and 1-D time," *IEEE Trans. Signal Proc.*, vol. 56, no. 8, pp. 3572–3585, 2008.
- [7] M. Püschel and J. M. F. Moura, "Algebraic signal processing theory: 1-D space," *IEEE Trans. Signal Proc.*, vol. 56, no. 8, pp. 3586–3599, 2008.
- [8] M. Püschel and J. M. F. Moura, "Algebraic signal processing theory: Cooley-Tukey type algorithms for DCTs and DSTs," *IEEE Trans. Signal Proc.*, vol. 56, no. 4, pp. 1502–1521, 2008.
- [9] A. Sandryhaila, J. Kovacevic, and M. Püschel, "Algebraic signal processing theory: 1-D Nearest-neighbor models," *IEEE Trans. on Signal Proc.*, vol. 60, no. 5, pp. 2247–2259, 2012.
- [10] A. Sandryhaila, J. Kovacevic, and M. Püschel, "Algebraic signal processing theory: Cooley-Tukey type algorithms for polynomial transforms based on induction," *SIAM J. Matrix Analysis and Appl.*, vol. 32, no. 2, pp. 364–384, 2011.
- [11] M. Jackson, *Social and Economic Networks*, Princeton Univ., 2008.
- [12] M. Newman, *Networks: An Introduction*, Oxford Univ. Press, 2010.
- [13] D. Easley and J. Kleinberg, *Networks, Crowds, and Markets*, Cambridge Univ. Press, 2010.
- [14] M. E. J. Newman, "Coauthorship networks and patterns of scientific collaboration," *Proc. Nat. Acad. Sci.*, vol. 101, pp. 5200–5205, 2004.
- [15] L. A. Adamic and N. Glance, "The political blogosphere and the 2004 U.S. election: Divided they blog," in *Proc. Int. Workshop on Link Discovery*, 2005, pp. 36–43.
- [16] S. Brin and L. Page, "The anatomy of a large-scale hypertextual web search engine," *Comp. Networks and ISDN Syst.*, vol. 30, pp. 107–117, 1998.
- [17] P. Lancaster and M. Tismenetsky, *The Theory of Matrices*, Academic Press, 2nd edition, 1985.
- [18] F. R. Gantmacher, *Matrix Theory*, vol. I, Chelsea, 1959.
- [19] M. Vetterli and J. Kovačević, *Wavelets and Subband Coding*, Signal Processing, Prentice Hall, Englewood Cliffs, NJ, 1995.
- [20] S. Mallat, *A Wavelet Tour of Signal Processing*, Academic Press, 3rd edition, 2008.
- [21] A. Bovik, *Handbook of Image and Video Processing*, Academic Press, 2nd edition, 2005.
- [22] "National Climatic Data Center," 2011, <ftp://ftp.ncdc.noaa.gov/pub/data/g sod>.
- [23] T. J. Rivlin, *An Introduction to the Approximation of Functions*, Dover Publications, 1969.
- [24] R. O. Duda, P. E. Hart, and D. G. Stork, *Pattern Classification*, Wiley, 2nd edition, 2000.
- [25] O. Chapelle, B. Schölkopf, and A. Zien, *Semi-Supervised Learning*, MIT Press, 2006.
- [26] L. I. Rudin, S. Osher, and E. Fatemi, "Nonlinear total variation based noise removal algorithms," *Physica D*, vol. 60, no. 1–4, pp. 259–268, 1992.
- [27] T. F. Chan, S. Osher, and J. Shen, "The digital TV filter and nonlinear denoising," *IEEE Trans. Image Proc.*, vol. 10, no. 2, pp. 231–241, 2001.
- [28] J. P. Oliveira, J. M. Bioucas-Dias, and M. A. T. Figueiredo, "Adaptive total variation image deblurring: A majorization-minimization approach," *Signal Proc.*, vol. 89, no. 9, pp. 1683–1693, 2009.
- [29] I. W. Selesnick and P. Chen, "Total variation denoising with overlapping group sparsity," in *Proc. IEEE Int. Conf. Acoust., Speech and Signal Proc.*, 2013.
- [30] D. Zhou, O. Bousquet, T. N. Lal, J. Weston, and B. Schölkopf, "Learning with local and global consistency," in *Proc. Neural Inf. Proc. Syst.*, 2004, pp. 321–328.
- [31] M. Belkin, I. Matveeva, and P. Niyogi, "Regularization and semi-supervised learning on large graphs," in *Proc. Conf. Learn. Th.*, 2004, pp. 624–638.
- [32] F. Wang and C. Zhang, "Label propagation through linear neighborhoods," in *Proc. Int. Conf. Mach. Learn.*, 2006, pp. 985–992.
- [33] F. R. K. Chung, *Spectral Graph Theory*, AMS, 1996.
- [34] M. Belkin and P. Niyogi, "Laplacian eigenmaps for dimensionality reduction and data representation," *Neural Comp.*, vol. 15, no. 6, pp. 1373–1396, 2003.
- [35] U. Luxburg, "A tutorial on spectral clustering," *Stat. Comput.*, vol. 17, no. 4, pp. 395–416, 2007.
- [36] D. K. Hammond, P. Vandergheynst, and R. Gribonval, "Wavelets on graphs via spectral graph theory," *J. Appl. Comp. Harm. Anal.*, vol. 30, no. 2, pp. 129–150, 2011.
- [37] A. Agaskar and Y. Lu, "A spectral graph uncertainty principle," Submitted for publication., June 2012.
- [38] X. Zhu and M. Rabbat, "Approximating signals supported on graphs," in *Proc. IEEE Int. Conf. Acoust., Speech and Signal Proc.*, 2012, pp. 3921–3924.
- [39] S. K. Narang and A. Ortega, "Perfect reconstruction two-channel wavelet filter banks for graph structured data," *IEEE Trans. Signal Proc.*, vol. 60, no. 6, pp. 2786–2799, 2012.
- [40] D. I. Shuman, S. K. Narang, P. Frossard, A. Ortega, and P. Vandergheynst, "The emerging field of signal processing on graphs," *IEEE Signal Proc. Mag.*, vol. 30, no. 3, pp. 83–98, 2013.
- [41] Y. LeCun, L. Bottou, Y. Bengio, and P. Haffner, "Gradient-based learning applied to document recognition," *Proc. IEEE*, vol. 86, no. 11, pp. 2278–2324, 1998.